Supporting Information

Artificially tailored functional layer on Li-rich layer cathodes enables stable

high-temperature interphase for Li-ion batteries

Yaru Yang[a, 1], Gang Sun[a, b, 1,*], Qingjun Zhu[a], Yunshan Jiang[c], Wang ke[c], Panpan Wang[a],

Yang Zhao[d], Wang Zhang[a], Zhenbo Wang[a, b, c, *]

[a] College of Materials Science and Engineering, Shenzhen University, Shenzhen 518071, China,
Email:
[b] College of Physics and Optoelectronic Engineering, Shenzhen University, Shenzhen 518060,
China
[c] MIIT Key Laboratory of Critical Materials Technology for New Energy Conversion and Storage,
State Key Lab of Urban Water Resource and Environment, School of Chemistry and Chemical
Engineering, Harbin Institute of Technology, No.92 West-Da Zhi Street, Harbin 150001, China,
Email: wangzhb@hit.edu.cn;
[d] Department of Mechanical and Materials Engineering, University of Western Ontario, London,
Ontario, N6A 5B9, Canada

[*]**Corresponding author:** E-mail address: sgang2@szu.edu.cn (G. Sun); wangzhb@hit.edu.cn (Z.B.
Wang)

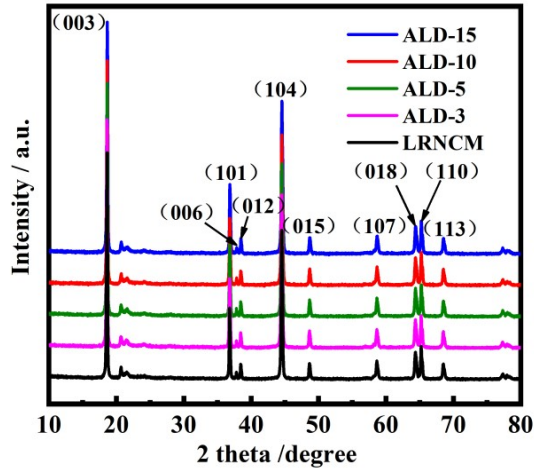1. Yaru Yang and Gang Sun contributed equally to this work.

Fig. S1. XRD patterns of the LRNCM, ALD-3, ALD-5.ALD-10 and ALD-15 samples.

Table. S1. The ICP test results of the LRNCM and ALD-10 samples.

Samples	Li	Mn	Ni	Co	Si
LRNCM	1.235	0.531	0.182	0.087	0
ALD-10	1.209	0.536	0.178	0.085	0.007

Table. S2. Summary of structural refinement of the LRNCM and ALD-10 samples by the Rietveld method.

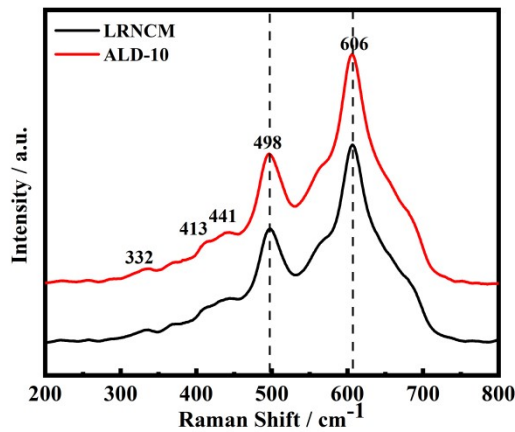| Samples	a=b	c	c/a
LRNCM	2.8832	14.3803	4.9876
ALD-10	2.8833	14.3805	4.9875

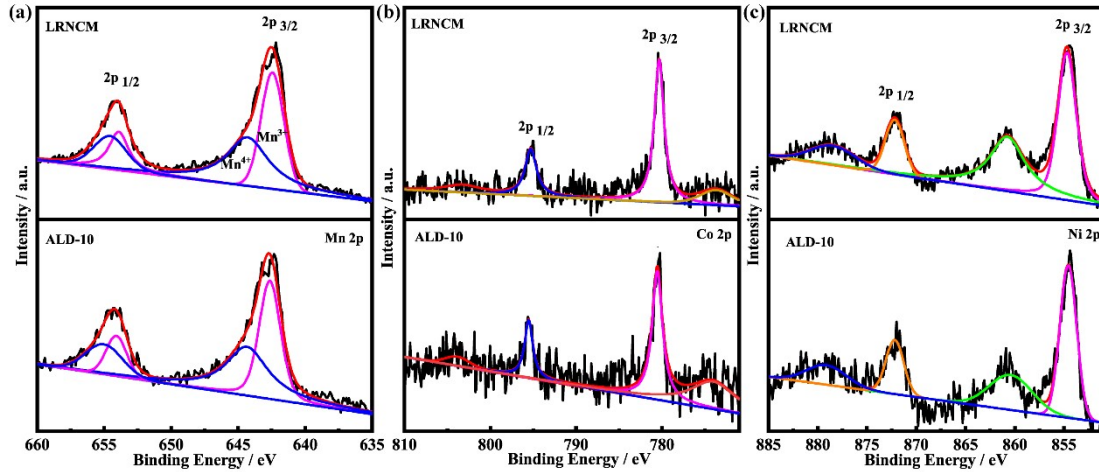Fig. S2. The Raman spectrum of the LRNCM and ALD-10 samples

Fig. S3. The core-level XPS spectrum of (a) Mn 2p, (b) Co 2p and (c) Ni 2p for the LRNCM and ALD-10 samples.

As can be seen from Fig. S3a, the Mn 2p spectra exhibited two main peaks Mn $2p_{3/2}$ and Mn$2p_{1/2}$, which are located at 642.4 eV and 654.5 eV in the LRNCM sample, whereas 642.6eV and 655.0 eV represent the Mn $2p_{3/2}$ and Mn $2p_{1/2}$ in the ALD-10 sample, respectively.[1,2] The result is in good agreement with the reported results of Mn^{4+}. For both samples in Fig. S3b, the Co $2p_{3/2}$ peaks are at 780.4 eV, which means the Co^{3+} ions. In Fig. S3c, the Ni 2p spectra confirm two main peaks of Ni $2p_{3/2}$ and Ni $2p_{1/2}$ around 854.7 eV and 872.1 eV in the LRNCM sample, whereas 854.4 eV and 872.1 eV represent the Ni $2p_{3/2}$ and Ni $2p_{1/2}$ in the ALD-10 sample, respectively. In addition, 860.7 eV and 872.1 eV represent satellite peaks in the LRNCM sample, and strong satellite peaks near Ni $2p_{3/2}$ and Ni $2p_{1/2}$ in ALD-10 samples are located at 860.4 eV and 872.1 eV. In principle, the energy difference of divalent cations is about 6.0 eV, and trivalent and tetravalent cations are about 10.0 eV. In this context, the energy difference value is 6.0 eV, indicating the Ni is at divalent cations Ni^{2+} both in LRNCM and ALD-10 samples. By XPS analysis, it can be concluded that the valences of Mn, Co, and Ni elements are similar between the two samples, investigating that the ALD

process has little effect on the oxidation state of Mn, Ni, and Co elements in the LRNCM.
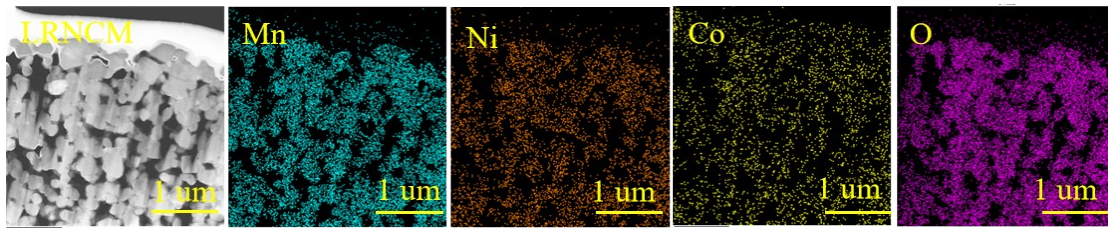

Fig. S4. The cross-section FIB/TEM images with the EDS mappings of the LRNCM sample.
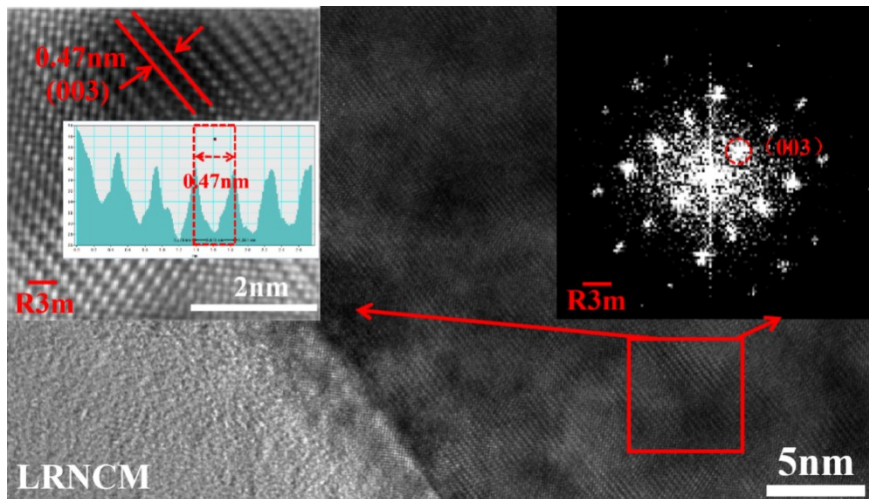

Fig. S5. The HRTEM, corresponding IFFT, and FFT images of the LRNCM sample.
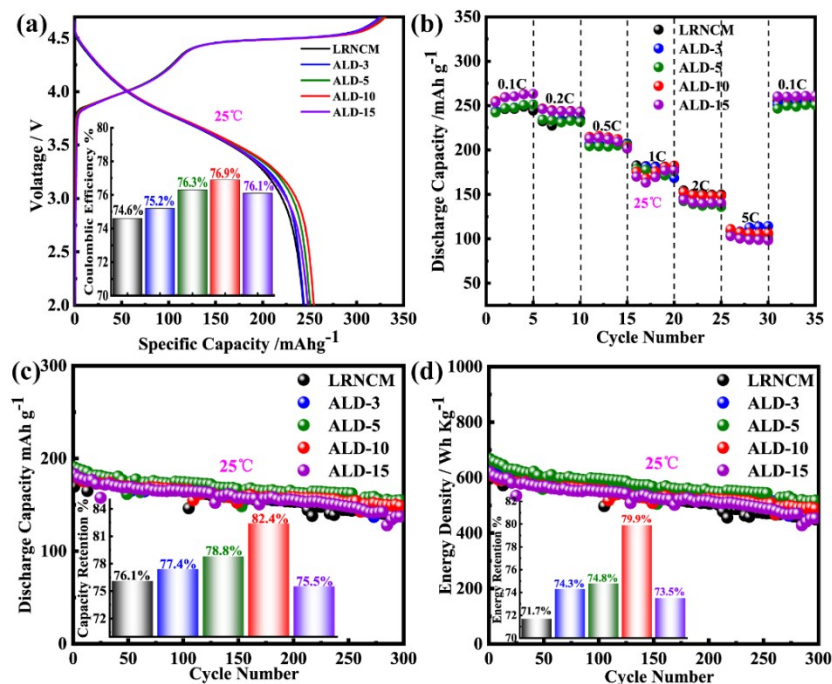
Fig. S6. (a) The initial charge-discharge profiles of LRNCM, ALD-3, ALD-5, ALD-10, and ALD-15 samples at 0.1 C in the range of 2.0–4.7 V at 25°C; (b) Rate performance of LRNCM, ALD-3, ALD-5.ALD-10 and ALD-15 samples at 25°C; (c, d) Cycle performance (c) and energy density (d) of LRNCM, ALD-3, ALD-5.ALD-10 and ALD-15 samples were at 1 C, 25°C, and 2.0–4.7 V.

The first charge capacities of the LRNCM, ALD-3, ALD-5, ALD-10 and ALD-15 samples in Fig. S6a are 326.2, 324.5, 327.9, 330.6, and 325.6 mAh g^{-1}, and the corresponding first discharge-specific capacities were 243.4, 244.1, 250.5, 254.5, and 247.9 mAh g^{-1}, with the corresponding ICE being 74.6%,75.2%,76.3%,76.9 and 76.1% at 25℃, respectively. Compared with the bare LRNCM, the ALD-treated samples show better ICE in inset Fig. S6a. These five samples have a difference at a higher cutoff voltage (over 4.5 V) in the charging process. As the cycles of ALD increase from 3 to 15, charge-specific capacity increases first and then decreases. When the cycles of ALD increased to 15 cycles, the first charge-discharge capacity and initial Coulombic efficiency of the ALD-15 sample dramatically decreases, which probably hinders the rapid intercalation and deintercalation of lithium ions (Li$^+$) due to the overly thick coating. The rate and cycle performance of the LRNCM and modified samples at

different current densities and 25°C is shown in Fig. S6b, c, and d. As shown in Fig. S6b, the discharge-specific capacities of the LRNCM sample were 246.4, 233.8, and 205.8 mAh g^{-1} at 0.1C, 0.2C, and 0.5C respectively, and the ALD-3 sample displays 247.3, 231.5 and 206.7 mAh g^{-1} at the corresponding rates, while other samples show 247.5, 231.2 and 203.8 mAh g^{-1} of the ALD-5 sample and 260.4, 243.7 and 212.1 mAh g^{-1} in the ALD-15 sample. However, the ALD-10 sample delivers higher discharge capacities of 260.5, 244.1, and 214.7 mAh g^{-1} at the related rates. Therefore, the ALD surface-modified LRNCM cathode influences improving rate performances, and the ALD-10 sample depicts the best rate performances, indicating that the over-thickened coating layer may be an obstacle to the kinetic transport of Li-ion. Cycling stability is verified at 1C from 2.0 to 4.7V at 25°C and the data is shown in Fig. S6c and S6d. The discharge-specific capacities of LRNCM, ALD-3, ALD-5, ALD-10 and ALD-15 samples after 300 cycles were 137.8, 143.9, 150.2, 148.7, and 138.4 mAh g^{-1}, with the corresponding capacity retention to be 76.1%, 77.4%, 78.8%,82.4% and 75.5% in Fig. S6c at 25°C, respectively. As shown in Fig. S6d, the energy density of LRNCM, ALD-3, ALD-5, ALD-10 and ALD-15 samples after 300th cycles were 448.9, 483.7, 499.3, 487.5, and 456.4Wh kg^{-1}, with the corresponding energy retention to be 71.7%, 74.3%, 74.8%, 79.9% and 73.5% at 25°C, respectively. These results show that the LRNCM electrode coated with 10 ALD cycles (ALD-10) has superior performance, compared with other cycle numbers of the ALD. The ALD surface modification strengthens the cycle stability since the direct ALD surface process suppresses the parasitic reactions between the LRNCM electrode and electrolyte.
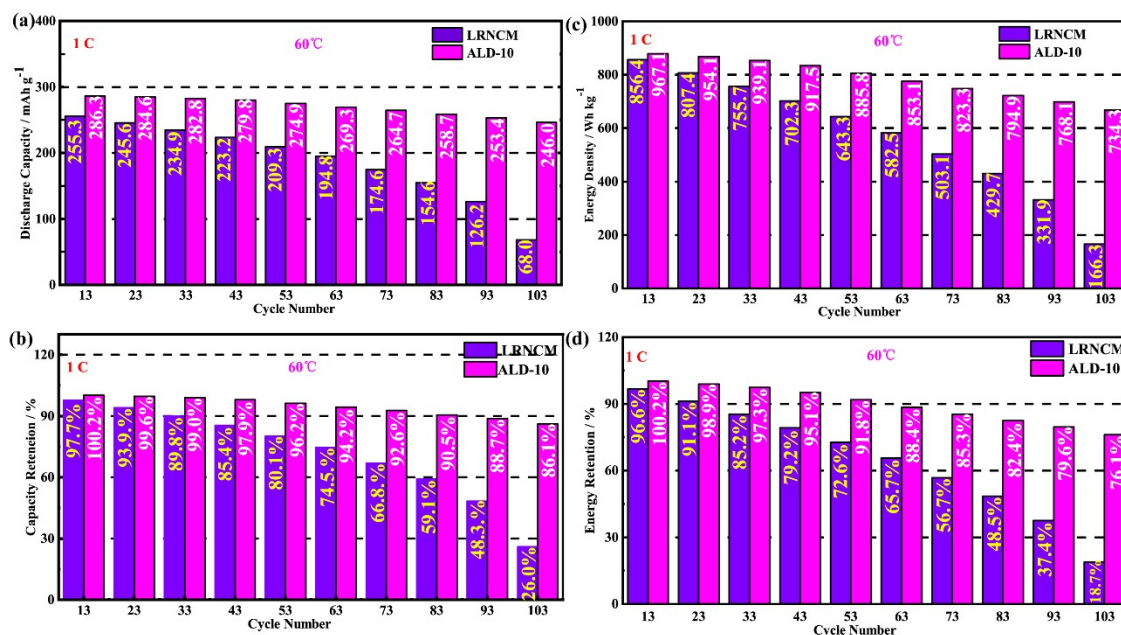
Fig. S7. The performance of discharge capacity (a) and energy density(b), capacity retention(c), and energy retention(d) of the LRNCM and ALD-10 samples every 10 cycles during the cycling tests at 1 C, 60°C, and 2.0–4.8 V (Constant current and constant voltage test).

Cycling performances of the LRNCM and ALD-10 samples are evaluated at 1 C in the voltage range of 2.0-4.8 V at 60°C as shown in Fig. S7. Both the LRNCM and ALD-10 samples exhibit relatively close capacity and energy retention at 13 cycles in Fig. S7b and 7d. But after 13 cycles, the capacity and energy decay decelerate dramatically in the LRNCM sample, due to the layered-to-spinel phase transforming dramatically and various interface side reactions increasing at high temperatures. However, after the Li_2SiO_3 coating layer by ALD, the cathode materials exhibit a significant improvement in energy retention (76.1%) and maintain 734.3Wh kg^{-1} after 100 cycles at 60°C in Fig. 7c, which is four times the 166.3 Wh kg^{-1} (18.7% energy retention) of the LRNCM sample. The prominent cycling performance may be related to the corrosion resistance of the Li_2SiO_3 coating layer on the cathode surface in extreme environments.
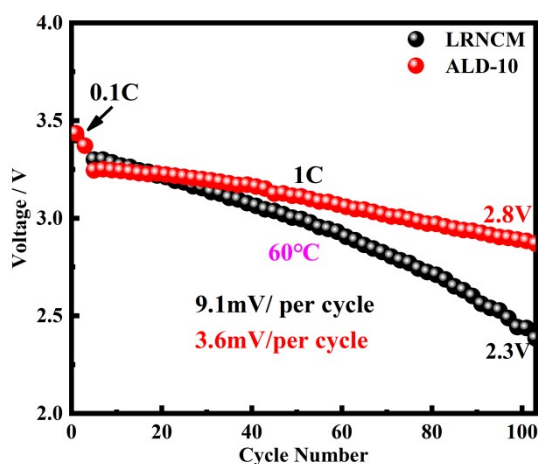
Fig. S8. The average discharge voltage of the LRNCM and ALD-10 samples is at 1 C, 60°C, and 2.0–4.8 V.

Fig. S8 shows the variation in discharge voltage. The voltage decay is 9.1 mV per cycle for the LRNCM electrode, which is almost triple that of the ALD-10 sample (3.6 mV per cycle). Both the LRNCM and ALD-10 samples exhibit an initial voltage of about 3.4V at 1C and similar voltage attenuation before the 25th cycle. But after the 25th cycle, the voltage decay dramatically. Fundamentally, the initial voltage decay before the 25th cycle is based on polarization. However, after the 25th cycle, the severe phase transition and complex interface reactions increase are the prominent reason leading to the fast voltage decay of the LRNCM sample at high temperatures. The LSO-ALD surface-modified LRNCM sample exhibits a remarkable improvement in voltage retention and maintains 2.8 V after 100th cycles at 60°C, and the value of the LRNCM electrode is only 2.3 V. This may be closely attributed to the robust and uniform protective film, which apply a prominent contribution to inhibiting the complex interface side reactions between the electrode surface and acidic electrolyte at high temperature.
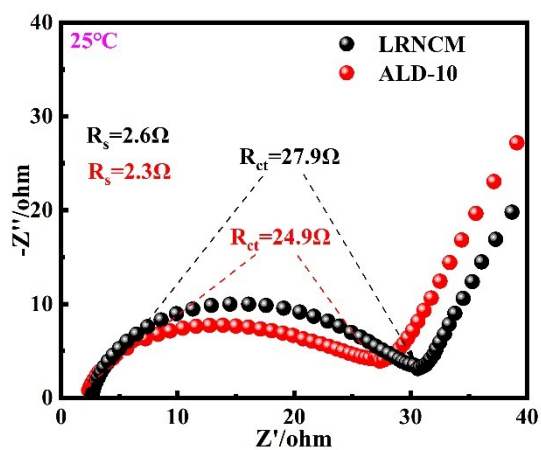
Fig. S9. EIS curves after the 5th cycle at 0.1C at 25℃ for LRNCM and ALD-10.
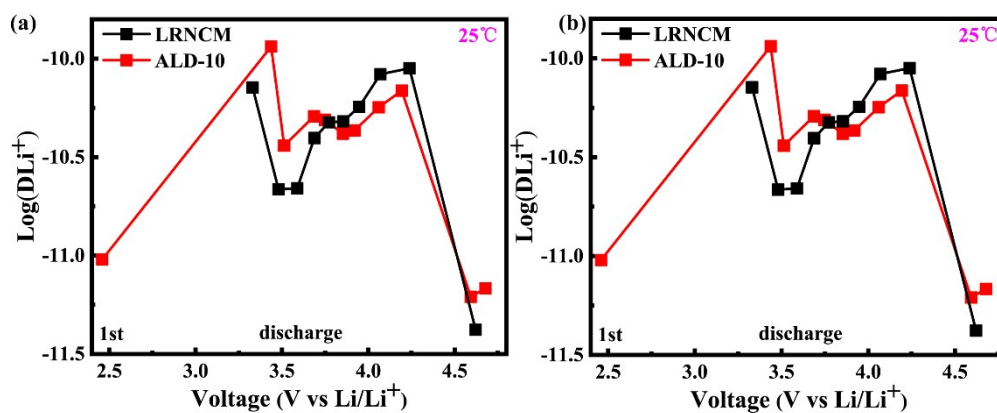

Fig. S10. The Li-ion diffusion coefficient was obtained from the charge(a) and discharge(b) processes of GITT.
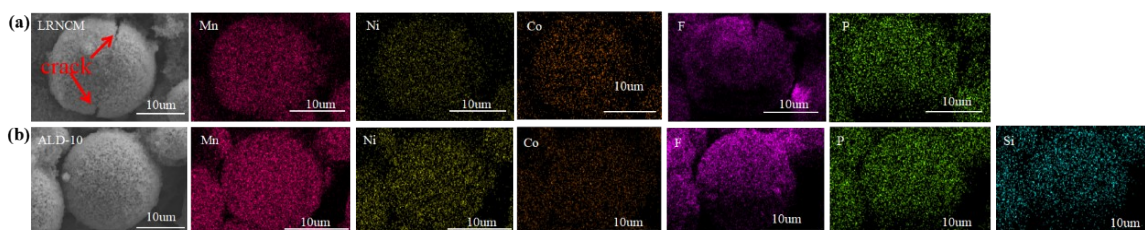

Fig. S11. SEM/EDS mappings of the cycled LRNCM(a) and ALD-10 (b) samples.
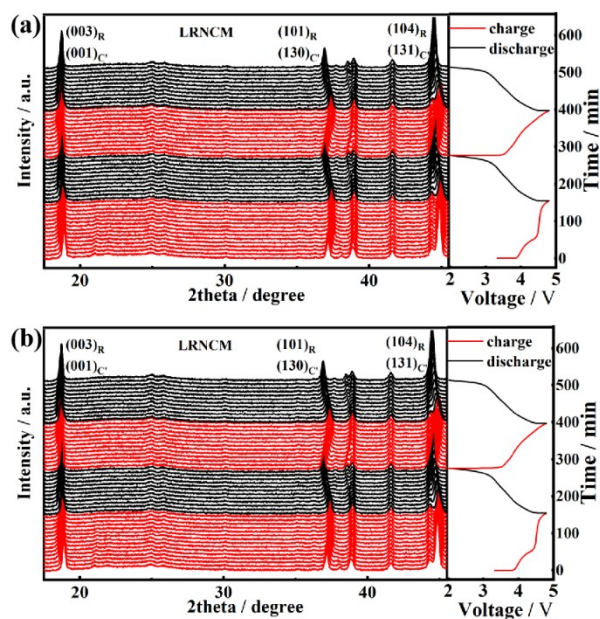
Fig. S12. The *in-situ* XRD curves and corresponding charge/discharge profile of the LRNCM (a) and ALD-10 (b) samples.
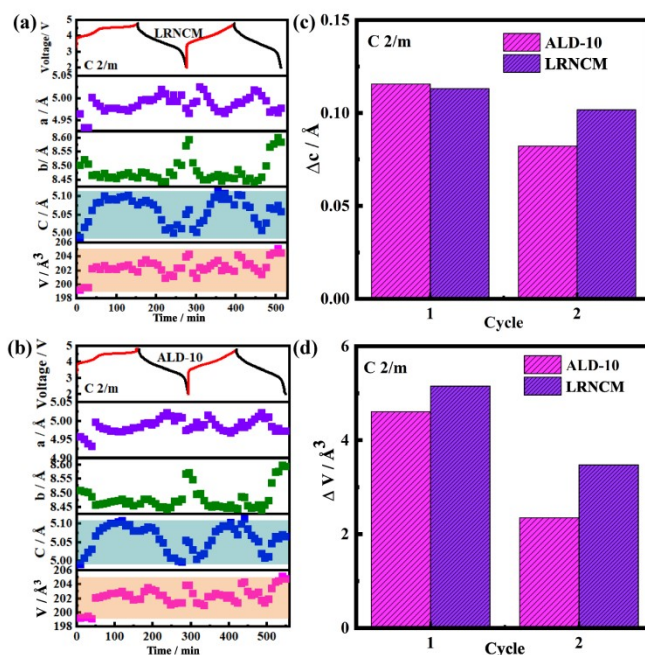

Fig. S13. Changes of lattice parameters during the first two cycles of the LRNCM(a) and ALD-10(b) samples; The corresponding lattice parameters $\triangle c$ and $\triangle V$ of the LRNCM(c) and ALD-10 (d) samples during the first two cycles.

The changes in lattice parameters during the first two cycles of the two samples are shown in Fig. S13a and 13b, and the corresponding lattice parameters $\triangle c$ and $\triangle V$ are shown in Fig. S13c and 13d. For the LRNCM sample, the maximum volume is 205.06 Å^3 and the minimum volume is 199.13 Å^3 during the first two cycles and the

volume change rate is 5.93%, while the unit cell volume change of the ALD-10 sample is between 199.21 Å^3 and 205.06 Å^3 and the volume change is 5.85%. As a result, the smaller variation of lattice parameters and cell volume after the ALD process indicates superior structural stability during the transport of Li$^+$.

References

1 X. Fan, Y. Huang, H. Wei, L. Tang, Z. He, C. Yan, J. Mao, K. Dai and J. Zheng, *Adv. Funct. Mater.*, 2022, **32**, 2109421.
2 E. Zhao, M. Chen, Z. Hu, D. Chen, L. Yang and X. Xiao, *J. Power Sources*, 2017, **343**, 345-353.